nature energy

ARTICLES

https://doi.org/10.1038/s41560-022-01085-8

Check for updates

Collective wind farm operation based on a predictive model increases utility-scale energy production

Michael F. Howland[1]✉, Jesús Bas Quesada[2], Juan José Pena Martínez[2], Felipe Palou Larrañaga[2], Neeraj Yadav[3], Jasvipul S. Chawla[3], Varun Sivaram[3,4] and John O. Dabiri[5,6]

In wind farms, turbines are operated to maximize only their own power production. Individual operation results in wake losses that reduce farm energy. Here we operate a wind turbine array collectively to maximize array production through wake steering. We develop a physics-based, data-assisted flow control model to predict the power-maximizing control strategy. We first validate the model with a multi-month field experiment at a utility-scale wind farm. The model is able to predict the yaw-misalignment angles which maximize array power production within ± 5° for most wind directions (5–32% gains). Using the validated model, we design a control protocol which increases the energy production of the farm in a second multi-month experiment by 3.0% ± 0.7% and 1.2% ± 0.4% for wind speeds between 6 m s^{-1} and 8 m s^{-1} and all wind speeds, respectively. The predictive model can enable a wider adoption of collective wind farm operation.

With consensus that carbon-intensive energy generation has contributed to global warming[1], the decarbonization of electricity production is of paramount importance[2]. Renewable energy must produce more than 60% of the primary energy supply by 2050 to achieve the 2 °C warming target set by the Paris Agreement[3]. Just 14% of worldwide energy production in 2015 was from renewables[3]. Meanwhile, the United States has set a goal of 100% carbon-free electricity generation by 2035[4], with similar international goals elsewhere[5]. Further, approaches to maximize renewable energy production in emerging economies are critical to address climate change[6]. Improvements in the efficiency of wind generation will enable a more rapid and lower-cost transition to a decarbonized energy system[7].

While individual horizontal axis wind turbines are approaching theoretical peak efficiency[8], wind farms exhibit losses from turbine interactions. Utility-scale wind farms can lose 10–20% of their energy production per year due to wake interactions between turbines[9]. Individual turbines generate turbulent, energy-deficit wake regions downwind[10]. Wind turbines are placed in close proximity to decrease the levelized cost of energy for the collective farm by reducing the capital costs[11]. The result is that modern turbines are spaced 6–10 rotor diameters apart in onshore wind farms[12], which results in substantial wake interactions[13]. All utility-scale wind turbines are operated to maximize their individual power production[14]. Such control inherently neglects wake interactions between neighbouring turbines.

Individual wind turbine operation attempts to minimize the yaw angle of misalignment between the incident wind direction and the turbine rotor orientation[15]. We consider collective wind farm operation through wake steering control, wherein certain wind turbines in the wind farm are intentionally misaligned in yaw with respect to the incident wind direction. The power production of the yaw-misaligned wind turbine is generally reduced, because the wind velocity perpendicular to the rotor is reduced[16]. The power production for the waked turbine may be increased due to wake deflection associated with the yawed turbine[17].

The goal of wake steering optimization in this study is to select the yaw-misalignment angles that maximize the power production of the wind farm by achieving increases in the power production of downwind turbines that compensate for the loss in power of the yaw-misaligned upstream turbines. Wake steering also affects loads and fatigue in the wind farm[18]. Wake steering can either increase or decrease fatigue in several ways, including potentially modifying turbine yaw duty, the incident turbulence intensity to waked turbines, wind turbine blade-bending moments and wind turbine torsional moments. While this study is focused on maximizing power, and loads are not directly considered in the optimization objective function, the empirical impact of the wake steering control on the determinants of turbine loads are measured and discussed. The power-maximizing yaw-misalignment angles inherently depend on the site-specific wind farm layout[19] and incident wind conditions[20,21], which vary in time. Therefore, the yaw optimization needs to be performed for each possible state of wind conditions[22], which is high-dimensional.

Because computational fluid dynamics simulations remain intractable for such optimization[23], the optimization of the yaw angles is generally performed with numerically efficient flow control wake models[24]. To remain tractable for optimization, wake models neglect certain flow physics[25] and parameterize the effects of turbulence in the wind farm and the atmospheric boundary layer (ABL)[26]. Using a wind farm operational strategy resulting from the optimization of a wake model has demonstrated potential to increase wind farm power production in large eddy simulations of idealized ABL conditions[21,24,27] and wind tunnel experiments[28,29].

[1]Civil and Environmental Engineering, Massachusetts Institute of Technology, Cambridge, MA, USA. [2]Siemens Gamesa Renewable Energy Innovation & Technology, Sarriguren, Spain. [3]ReNew Power Private Limited, Gurugram, India. [4]Office of the US Special Presidential Envoy for Climate, US Department of State, Washington, DC, USA. [5]Graduate Aerospace Laboratories (GALCIT), California Institute of Technology, Pasadena, CA, USA. [6]Department of Mechanical and Civil Engineering, California Institute of Technology, Pasadena, CA, USA. ✉e-mail: mhowland@mit.edu

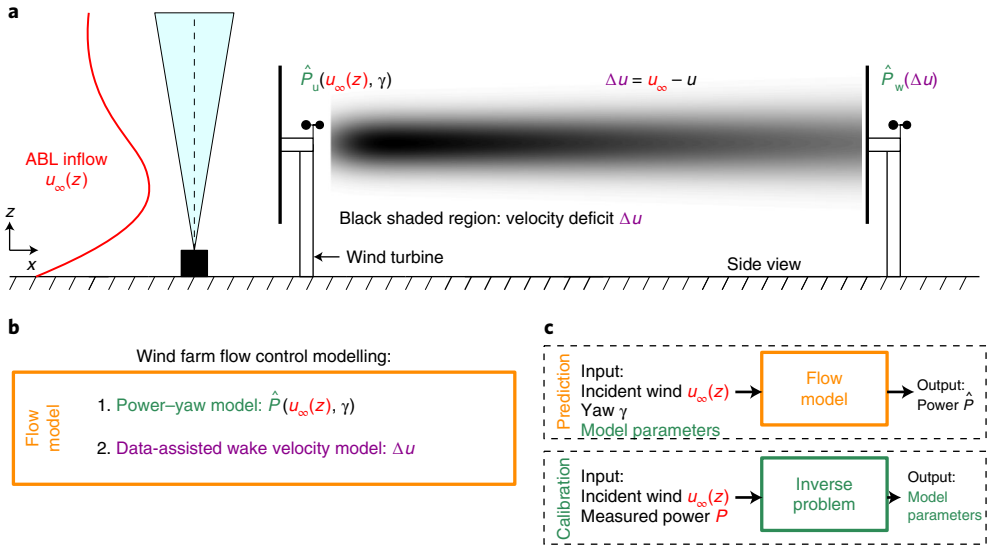

Fig. 1 | Schematic of the predictive wind farm flow control model. a, The ABL velocity profile is illustrated in red. Incident ABL winds $u_\infty(z)$ are measured in the field experiments using a LiDAR (Light Detection And Ranging, black box and blue cone). Each turbine is equipped with cup and sonic anemometers (black circles) and generates a wake region (black shaded region). To predict the effect of a control strategy on the power of the collective wind farm, we model the power production of upwind turbines operating in freestream conditions, $\hat{P}_u$, and the waked turbines, $\hat{P}_w$. **b**, The flow control model proposed in this study is the combination of a power–yaw model $\hat{P}(u_\infty(z), \gamma)$, which predicts the power production of a yawed turbine based on the incident wind $u_\infty(z)$ and the yaw-misalignment γ, and a data-assisted wake model, which predicts the wake velocity deficit Δu. The power–yaw model and the wake model are described in Supplementary Methods. **c**, The wake velocity model parameters are calibrated using wind farm data for which the turbines are operating in baseline, yaw-aligned conditions, $\boldsymbol{\gamma} = 0$. The wake model is then used to predict the farm power given a yaw control strategy, $\boldsymbol{\gamma} \neq 0$.

Initial field experiments of collective wake steering operation at utility-scale wind farms implemented operational strategies that are based on the optimization of a flow control model[19,30–32]. These studies have demonstrated that collective operation can increase power production for wind conditions that result in high wake losses, compared with standard individual control. However, to achieve the maximum power production of the wind farm, the flow control models must reliably predict the power-maximizing control strategy. It has not yet been demonstrated, using field data, that flow control models are able to predict the control strategy which maximizes power for utility-scale wind farms, because this requires both an accurate predictive flow model and a field experiment with sustained operation in suboptimal strategies.

In this study, we develop a methodology for operating wind turbines collectively to maximize wind farm energy production based on a predictive wind farm flow control model. We develop a predictive wind farm flow control model (Methods) that predicts the power production of each turbine within a wind farm based on the incident wind conditions and the control strategy of each individual turbine. The flow control model predicts the power production of upwind turbines given their operational strategy and given the measured incident ABL wind profiles[16] and predicts the power production of the downwind turbines using an analytical wake model[19,33,34] and leveraging data-driven parameter estimation techniques[35]. The modelling framework is described in Fig. 1. We then design and implement a field experiment at a commercial wind farm in India where we intentionally yaw misalign a wind turbine with a rotor diameter of approximately 120 m using fixed yaw angles between −25° and 25°. Importantly, we conduct our experiments in configurations predicted to result in optimal performance and suboptimal regimes. This enables direct validation of the flow control model predictions. Considering the yaw angles between −25° and 25°, we show that the proposed flow control model (Fig. 1) is able to predict the yaw-misalignment angles for the farm which maximize power production to within ±5° for most (4/6) conditions tested. Further, the model predicts the power-maximizing yaw angles within ±10° for 5/6 cases and the power-maximizing yaw direction for all cases (6/6). Leveraging the validated flow control model, we design a wake steering protocol wherein the yaw-misalignment angles of the wind farm vary according to the incident wind conditions. We then perform a second field experiment where we implement the power-maximizing wake steering protocol. We demonstrate a 1.2% ± 0.4% energy increase for the utility-scale wind farm for the wind directions of interest, compared with standard individual control.

Collective wind farm control field experiment

The wind farm (Fig. 2a) consists of approximately 100 turbines and is located in northwest India. The turbines are approximately 100 m in hub height and approximately 2 MW in capacity. We consider a subset of four turbines shown in Fig. 2b. We focus our experiment on turbines 1, 2 and 3. An adjacent freestream turbine is used as a reference and is labelled as 'Ref' (Fig. 2b). The turbines are approximately aligned for northwesterly inflow ($\alpha \approx -5°$). The prevailing wind conditions during the summer and winter are southwesterly and northeasterly, respectively, with spring and autumn as shoulder seasons with transitional winds. We focus our experiment on the northeasterly winter winds (Fig. 2c) because the southwesterly summer winds exhibit heterogeneous upwind blockage effects, which limit the potential to perform controlled experiments. The flow is statically stable, where buoyancy suppresses turbulence, and unstable, where buoyancy contributes to turbulence, approximately 70% and 30% of the time, respectively, for the inflow wind directions of interest for wake steering in this study ($-30° < \alpha < 45°$, stability estimation in Supplementary Note 1).

We first focus on assessing the fidelity of the flow model in predicting the wake steering control strategy, $\boldsymbol{\gamma}^*$, which maximizes power production. To achieve this, we implement a yaw-misalignment offset series for upwind turbine 1 (Fig. 2b), which operates in freestream conditions. We misalign turbine 1 for yaw values between −25° and

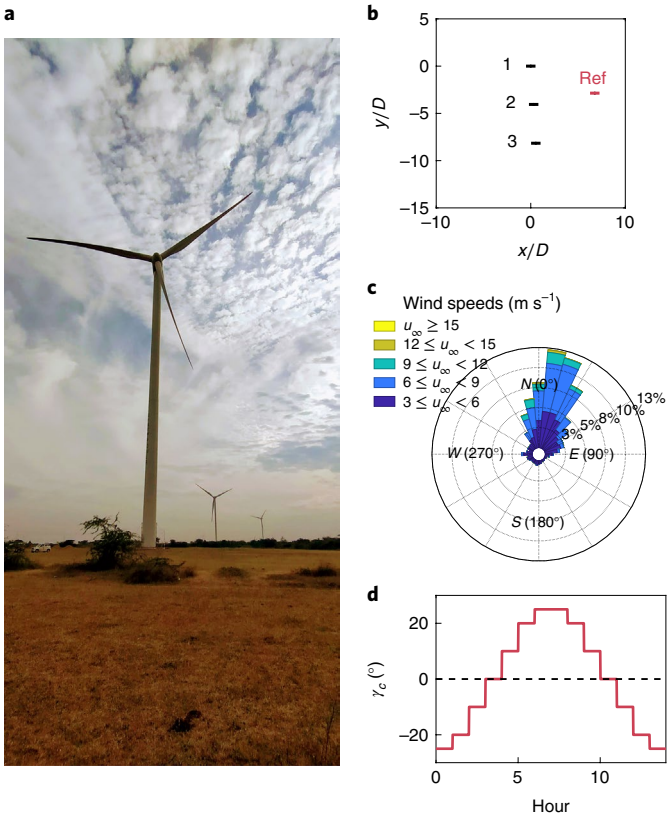

Fig. 2 | Collective wind farm operation experimental setup. a, Photo of the utility-scale wind farm of interest in this study, which is located in northwest India. **b**, Top view of the wind turbines of interest with the coordinates of the farm normalized by the wind turbine rotor diameter, *D*. The *x* and *y* directions correspond to easting and northing, respectively. The adjacent reference turbine is denoted as 'Ref'. **c**, Measured wind rose during the experimental period as recorded by the reference wind turbine. The radial distance from the centre corresponds to the probability of the wind speed and wind direction in the wind rose, given as percentages. **d**, Commanded yaw-misalignment sequence, γ_c, for the fixed yaw-misalignment flow control model validation experiment. The commanded yaw misalignments do not depend on the incident wind conditions. During the model validation experiment, each commanded yaw-misalignment value is held fixed for 1 h.

25° (Fig. 2d). Each yaw-misalignment set point is held fixed for 1 h and does not change depending on the incident wind conditions. Because the wind conditions vary in time, the fixed yaw set points will often result in suboptimal operation. We performed the model validation experiment from February 2020 until April 2020.

We consider the power production of the three-turbine array for incident wind speeds in Region II of the power curve (Region II consists of operation where wind turbines maximize their coefficients of power[36], nominally between 5 m s^{-1} and 9 m s^{-1} for the turbines of interest). The data-filtering methodology is described in Methods. We normalize the power production for each turbine at each 1 min averaged instance by the power production of the adjacent reference turbine to minimize the effect of the finite wind speed bin width and the cubic dependence of power on the wind speed. The model is calibrated using equation (2) for instances in which turbine 1 commands zero yaw, $\gamma_1 = 0°$. Given the calibration based on standard control, the model is then used to predict the power production given the various yaw-misalignment angles that were implemented for turbine 1 (Fig. 2d).

We first consider northerly incident wind ($\alpha = 0°$) for which the three-turbine array is slightly offset from alignment. Both the measured and model-predicted power for yaw misalignments of $\gamma_1 = -20°$, $\gamma_1 = +20°$ and yaw-aligned operation, $\gamma_1 = 0°$, are shown in Fig. 3. For baseline operation ($\gamma_1 = 0°$), the powers of turbines 2 and 3 are approximately 40% of the power of turbine 1 (Fig. 3e).

Our model predicts that negative yaw misalignment would reduce the array power production compared with baseline yaw-aligned control as the wake of turbine 1 will be steered towards the downwind turbines (Fig. 3a). Overall, a negative yaw misalignment of $\gamma_1 = -20°$ reduces the sum of power production for the three turbines by 5.1%. The power production for turbine 1 decreases due to its yaw misalignment. The power production for turbine 2 slightly increases due to the reduction of the thrust of turbine 1. The power production for turbine 3 is decreased for $\gamma_1 = -20°$, compared with $\gamma_1 = 0°$.

The wake model velocity and power production predictions for $\gamma_1 = +20°$ and $\alpha = 0°$ are shown in Fig. 3c,f, respectively. For $\gamma_1 = +20°$, the measured power productions for the downwind turbines 2 and 3 are statistically significantly higher than for $\gamma_1 = 0°$, as indicated by the 95% confidence intervals. Interestingly, the power for turbine 1 is slightly higher with positive yaw misalignment, compared with yaw-aligned operation for both field measurements and model predictions. This slight increase has been observed in other studies, depending on the incident wind conditions and turbine control system[16,31]. The slight power increase observed here is caused by a combination of clockwise wind direction turning with increasing height in the ABL, complex wind speed profiles with a subgeostrophic wind speed maximum in the rotor area and positive yaw misalignment (Supplementary Note 1 and Supplementary Figs. 5 and 6). Collectively, the yaw misalignment of turbine 1 to $\gamma_1 = +20°$ increased total power for the three-turbine array by 28.6%.

The wake model predictions for all three yaw-misalignment conditions shown in Fig. 3 are within or nearly within the 95% confidence intervals of the field data, validating the predictive accuracy of the flow control model proposed in this study. An outstanding question is whether the model can predict the yaw-misalignment values which maximize power for the utility-scale wind farm. Here we have yaw-misaligned turbine 1 for values between $\gamma_1 = -25°$ and $\gamma_1 = 25°$ ($|\gamma_1| > 25°$ was not tested for load limitations[18]). The value of γ_1 that maximizes the array power depends on the wind direction α. We compare the values of γ_1 that maximize the array power in the utility-scale wind farm data to the values of γ_1 that maximize the power predictions from the flow control model for different inflow wind directions α (positive and negative α are northeasterly and northwesterly winds, respectively). The results for six different incident wind directions are shown in Fig. 4. The power for the individual turbines, depending on the incident wind direction and turbine 1 yaw misalignment are shown in Supplementary Note 1. The wake model predictions are within the 95% confidence intervals of the field data for 72% of the different combinations of wind direction α and yaw misalignment γ_1 (46/64). The value of γ_1 that maximizes power in the flow control model is within 5° of the value that maximizes power in the field data for 4/6 values of α. On the basis of the observed trend, it is possible that the power-maximizing yaw in field conditions is $|\gamma| > 25°$ for $\alpha = -7.5°$, but we do not have access to these data given the experimental setup and we do not expect $|\gamma^*|$ to be much greater than 30° given the high power loss at turbine 1 for large yaw in mean conditions[16], although the value of this power loss depends on the time-varying wind conditions. The results demonstrate that the flow control model is able to accurately estimate the power-maximizing yaw-misalignment angles in utility-scale wind farms with sufficient precision to implement wake steering given typical yaw set point lookup table resolutions (5°, ref. [16]).

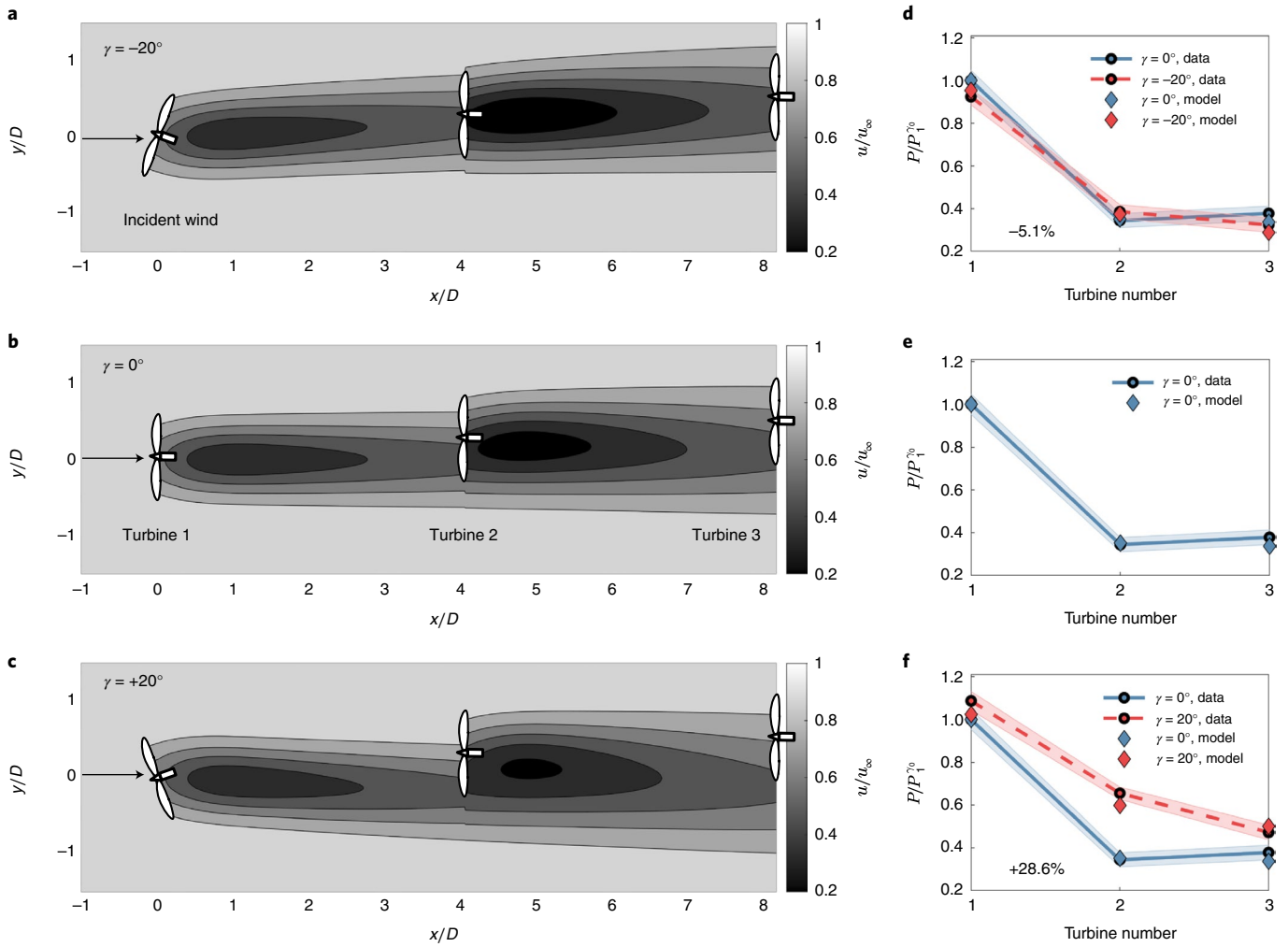

Fig. 3 | Model predictions and field experiment results from the static yaw-misalignment model validation field experiment for three yaw-misalignment values. a–c, Streamwise velocity contours predicted by the flow control model for turbine 1 yaw misalignments of $\gamma_1 = -20°$ (**a**), $\gamma_1 = 0°$ (**b**) and $\gamma_1 = 20°$ (**c**) are shown for wind directions α from the north between $0 \pm 2.5°$. The wind speed is $7 \pm 1.5\,m\,s^{-1}$ and the turbulence intensity is $5 \pm 2.5\%$, as measured by the reference turbine. To account for the finite wind speed bin width, the power for each 1 min averaged data sample for each turbine is normalized by the corresponding power of the adjacent reference turbine, and the normalized power is denoted as P. The yaw angles implemented in **a** and **c** are predicted to steer the wake region towards (**a**) or away (**c**) from the downwind turbines, depending on the yaw angle. Steering the wake away from the downwind turbines (**c**) is predicted to increase array power production (power prediction in **f**). **d–f**, Comparison of the wake model predictions to the measured power production for the three-turbine array for turbine 1 yaw misalignments of $\gamma_1 = -20°$ (**d**), $\gamma_1 = 0°$ (**e**) and $\gamma_1 = 20°$ (**f**). The powers are normalized by the power production of the leading turbine 1 with $\gamma_1 = 0°$ ($P/P_1^{\gamma 0}$) so that the results can be interpreted as a fractional gain in power compared with baseline control. The field experiment measurements are shown as circles, and the model predictions are shown as diamonds. The shaded region corresponds to 95% confidence intervals around the mean, estimated with bootstrapping. The blue and red correspond to yaw alignment and yaw misalignment, respectively. The flow control model is calibrated to the yaw-aligned data $\gamma_1 = 0°$. The flow control model is then used to predict the power production for yaw-misaligned operation. For this plot, the measured angular velocity is used in the power–yaw model. The effect of the turbine 1 yaw misalignment on power production of the waked turbines (2 and 3) depends on the direction (sign) of the yaw. The field experiment measurements demonstrate a −5.1% and +28.6% change in the three-turbine array mean power production compared with $\gamma_1 = 0°$ for $\gamma_1 = -20°$ and $\gamma_1 = +20°$, respectively. For $\gamma_1 = -20°$ (**d**), both the data and the predictive model result in a slight decrease in the power production of turbine 1 compared with $\gamma_1 = 0°$. For $\gamma_1 = +20°$ (**f**), both the data and the predictive model result in a slight increase in the power production of turbine 1 compared with $\gamma_1 = 0°$. This small gain is associated with the incident wind velocity profiles in the ABL which occurred during operation with $\gamma_1 = +20°$ (Supplementary Figs. 5 and 6); such a small gain has also been shown for certain flow conditions and yaw misalignments in previous studies[16,31].

While the flow control model predictions are within the field data confidence intervals for most combinations of wind direction and yaw misalignment, the flow control model generally slightly underpredicts the power increases from wake steering (Fig. 4). These underpredictions are the result of an underprediction of the power gain for turbine 2 given $\gamma_1 \neq 0$ (turbine-specific results in Supplementary Note 1). Future work is required to improve the predictive accuracy of optimization-oriented wake models, including the improved modelling of wake curling[37–39], veer[16,40] and stability[21,41].

Second, we focus on increasing the wind farm energy production through wake steering control. The optimal yaw-misalignment angles for the array depend on the incident wind conditions. Contrary to the first experiment, we dynamically adapt the

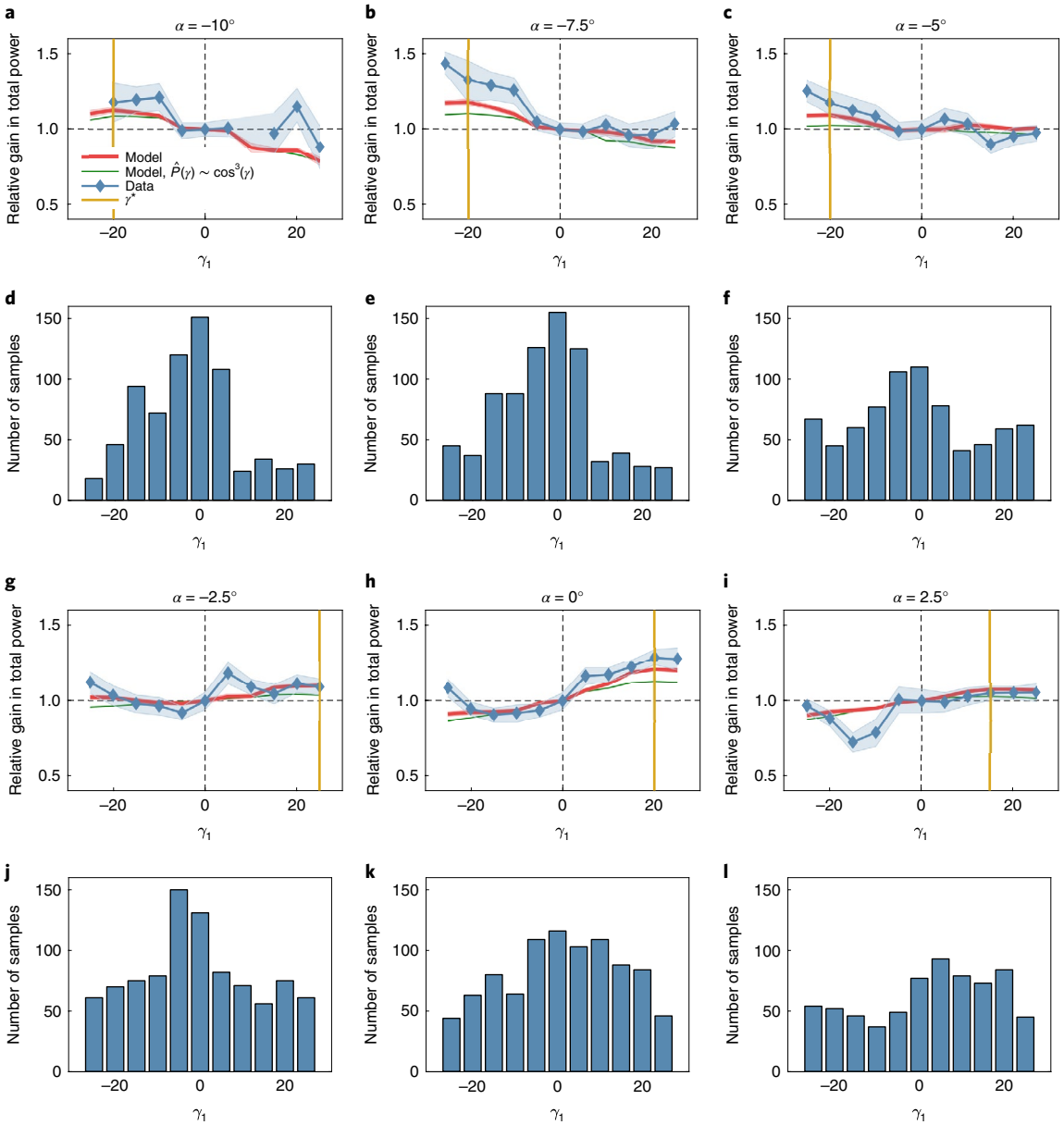

Fig. 4 | Results from the static yaw-misalignment field experiment for flow control model validation. The relative gain in the total power for turbines 1, 2, and 3 as a function of the yaw misalignment of turbine 1 from the static yaw-misalignment field experiment is shown, $\sum_i^{N_t} P_i(\gamma_1)/\sum_i^{N_t} P_i(\gamma_1 = 0)$ where $N_t = 3$ is the number of turbines and P_i is the power production of each turbine. The power and number of data samples are shown for different inflow wind directions, α, and yaw-misalignment angles, γ: **a**–**l**, $\alpha = -10°$ (**a**,**d**), $\alpha = -7.5°$ (**b**,**e**), $\alpha = -5°$ (**c**,**f**), $\alpha = -2.5°$ (**g**,**j**), $\alpha = 0°$ (**h**,**k**) and $\alpha = 2.5°$ (**i**,**l**). The yaw angles are shown in degrees. The origin corresponding to zero yaw misalignment is shown with dashed lines. The yaw-misalignment values tested were between −25° and 25° (yaw values beyond |25°| were not considered for loading limits). The wind turbines are approximately aligned for northwesterly inflow ($\alpha \approx -5°$). The power is normalized by the power produced with zero turbine 1 misalignment $\gamma_1 = 0°$ so that the results can be interpreted as a fractional gain in power compared with baseline control. The wind speed is $7 \pm 1.5\,m\,s^{-1}$, and the turbulence intensity is $5 \pm 2.5\%$, as measured by the reference turbine. To account for the finite wind speed bin width, the power for each 1 min averaged data sample for each turbine is normalized by the corresponding power of the adjacent reference turbine, and the normalized power is denoted as P. Conditional averages with $n > 25$ data samples are considered. In blue, we show the field experiment mean data with 95% confidence intervals from bootstrapping. Mean flow control model predictions with 95% confidence intervals from bootstrapping are shown in red. The flow control model predictions use the predicted wind turbine angular velocities. The power-maximizing yaw-misalignment angle for turbine 1 predicted by the flow control model is given in gold. Flow control model predictions assuming that the power production of yawed turbines is $\hat{P}(\gamma) \sim \cos^3(\gamma)$ are shown in green. The impact of the yaw misalignment of turbine 1 on the power of each of the three individual turbines of interest is shown in Supplementary Note 1 (Supplementary Figs. 3–9).

yaw-misalignment set points depending on the incident wind conditions to match γ^*, the model-optimal wake steering control strategy. We tabulate γ^* for three independent input variables: wind speed, wind direction and turbulence intensity. Details regarding the calibration and optimization of the flow control model are in the Supplementary Note 2. The model-optimal yaw-misalignment angle set points are applied to the wind turbine array based on the 5 min moving averaged wind conditions measured by the reference

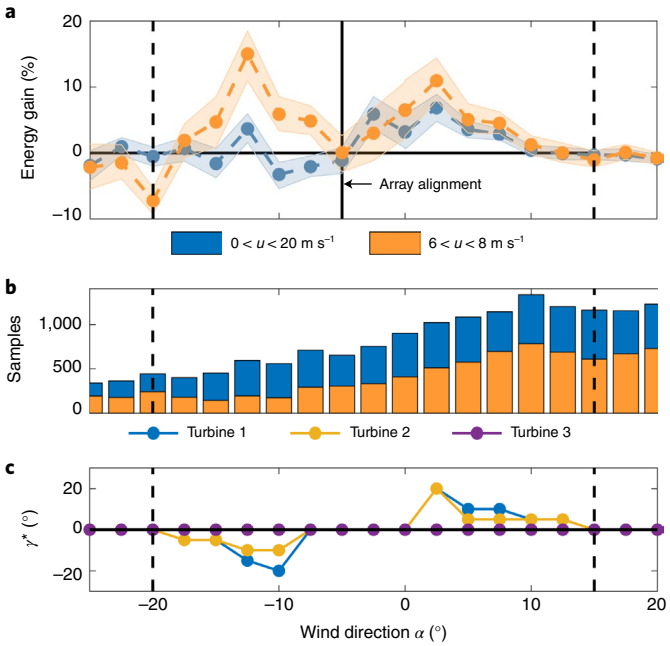

Fig. 5 | Results from utility-scale collective wind farm operation to maximize energy production. a, Energy gain from the farm energy maximization wake steering field experiment. The results for wind speeds between $6 < u < 8\,\mathrm{m\,s^{-1}}$ and $0 < u < 20\,\mathrm{m\,s^{-1}}$ (full wind speed range) are shown in orange and blue, respectively. The shaded region corresponds to 95% confidence intervals around the mean estimated with bootstrapping. The wind turbines are approximately aligned for northwesterly inflow ($\alpha \approx -5°$), shown with a solid black vertical line. The vertical dashed lines indicate the wind direction bounds for which collective operation is applied ($\gamma \neq 0°$), $-20° < \alpha < 15°$. **b**, Number of unique 1 min averaged data samples collected for each wind direction for wake steering operation. The number of data points collected for baseline yaw-aligned operation is similar. **c**, The yaw-misalignment set points applied to the farm, which maximize wind farm power production in the flow control model, γ^*, for each turbine. The power-maximizing yaw angles, γ^*, depend on the incident wind conditions of: wind speed, wind direction and turbulence intensity. The yaw angles for incident wind speeds of $5 \pm 1\,\mathrm{m\,s^{-1}}$ and turbulence intensities of $7.5 \pm 1.25\%$ are shown. The full yaw-misalignment lookup table is provided in the supporting dataset.

wind turbine. During this experiment, we construct datasets for the wind farm power production in both wake steering and baseline yaw-aligned control. We switch between wake steering control and baseline control every 2.5 h (experimental details in Methods). We performed the energy maximization experiment from December 2020 until March 2021.

We consider the impact of wake steering control on wind farm energy production. The previous experiment demonstrated that wake steering can increase or decrease power production, depending on the incident wind conditions and the prescribed yaw-misalignment values (Fig. 4). In this second experiment, we set the yaw-misalignment values for each turbine in the farm to the model-optimal result γ^* depending on the incident wind speed, direction and turbulence intensity. Wake steering control is active ($\gamma \neq 0$) for $-17.5° < \alpha < 12.5°$, because these are the wind directions with wake losses. Although the commanded yaw is zero outside of $-17.5° < \alpha < 12.5°$, our analysis considers $-20° < \alpha < 15°$ to account for hysteresis in the yaw controller[30].

The effect of wake steering on the array power production will depend on the prescribed yaw misalignment and the incident wind conditions. For example, we expect wake steering to have a relatively small effect on wind farm power production for high wind speeds (above the rated wind speed of the generator where power is constant at the rated power) because wake losses are relatively small. However, higher speeds contribute more to wind farm energy than lower speeds. To assess the collective benefit of wake steering, we assess the impact of wake steering on the array energy production. The gain in energy from wake steering control, compared with baseline individual control, is computed using equations (4)–(6) and is described in Methods.

Table 1 | Wind farm energy gain from collective wake steering operation over wind direction and wind speed sectors

Wind speed	Incident wind direction sector	
($\mathrm{m\,s^{-1}}$)	$-20° < \alpha < 15°$	$-180° < \alpha < 180°$
$6 < u < 8$	$+3.0\% \pm 0.7\%$	$+1.1\% \pm 0.4\%$
$0 < u < 20$ (full u range)	$+1.2\% \pm 0.4\%$	$+0.4\% \pm 0.3\%$

The uncertainty estimates are 95% confidence intervals from bootstrapping. The wind farm energy gain is estimated using equation (7) (Methods).

First, we consider the gain in energy for each independent wind direction. We first consider wind speeds between $6\,\mathrm{m\,s^{-1}}$ and $8\,\mathrm{m\,s^{-1}}$, the centre of Region II of the power curve, selected to ensure we do not cross into other control regions. These were the wind speeds of interest in the model validation experiment (Fig. 4). The energy gain from wake steering control is shown for each wind direction in Fig. 5a. The number of unique 1 min averaged data samples collected for wake steering operation for each α is shown in Fig. 5b (similar numbers of samples were collected for aligned control). Wake steering results in statistically significant gains in energy when active ($\gamma \neq 0$).

Considering the full wind speed range encountered ($0\,\mathrm{m\,s^{-1}}$ to $20\,\mathrm{m\,s^{-1}}$), the energy gain results are qualitatively similar although the magnitude of gain is decreased. This is expected because wake steering control will not be active for higher wind speeds (above rated), given limited wake losses. The energy gain from wake steering control decreased more for $\alpha < -5°$ than for $\alpha > -5°$. This decrease is primarily associated with an energy decrease for the simultaneously waked and yaw-misaligned turbine 2 at moderate wind speeds between 8 and $10\,\mathrm{m\,s^{-1}}$, as detailed further in Supplementary Note 3 (Supplementary Figs. 10–12).

We compute the energy gain over a sector of wind directions using equation (7) (Methods). The energy gains over two wind direction sectors for wind speeds between $6 < u < 8\,\mathrm{m\,s^{-1}}$ (Region II) are shown in Table 1. For Region II operation, wake steering has a statistically significant increase for both the incident wind directions where wake steering is active ($3.0\% \pm 0.7\%$) and the full wind direction distribution between $-180° < \alpha < 180°$ ($1.1\% \pm 0.4\%$). Because wake steering is active only for wind directions that lead to wake interactions, the degree to which wake steering increases total energy production depends on the fraction of time in which the wind is oriented in these directions. In this experiment, wake steering, which was active only between $-17.5°$ and 12.5°, increased energy to a sufficient degree that it resulted in a statistically significant increase in the energy production in Region II for the full wind direction distribution ($-180°$ to 180°).

The sector energy gains for the full wind speed range of $0 < u < 20\,\mathrm{m\,s^{-1}}$ are shown in Table 1. For the wind directions for which wake steering is active, the energy production increase due to wake steering is statistically significant ($1.2\% \pm 0.4\%$). For the full wind speed and direction range, the energy production gain in this experiment is $0.4\% \pm 0.3\%$.

The wake steering control method developed in this study focuses on maximizing wind farm energy production. Wake

steering control will influence the fatigue loads of the individual wind turbines in the farm through different mechanisms[18,24]; wake steering can either increase or decrease different turbine fatigue loads. To enable industry adoption of wind farm control, a detailed understanding of the effects of wake steering on wind turbine fatigue loads is important. Wake steering can affect the yawed turbine yaw duty, the turbulence intensity incident to waked turbines, turbine blade-bending moments, the waked turbines torsional moments in partial waking scenarios and other loads. Because turbulence intensity has a substantial impact on wind turbine loads[18,42], wake steering can potentially be used to reduce waked turbine loads by reducing the incident turbulence intensity. Waked turbines operating in a partial wake, where the wake overlaps partially with the downwind turbine rotor, exhibit increased torsion[24]. Because wake steering deflects wakes, it may be a mechanism to either increase or decrease the waked turbine torsion, depending on the turbine layout and the wake steering strategy.

While direct load measurements were not available during the present field experiments, direct measurements of the determinants of farm loads were recorded. Turbulence intensity is reported at each turbine of interest. Wake steering reduced the turbulence intensity incident to downwind, waked turbines. For example, for $\alpha = 0°$ and $\gamma_1 = +20°$, the turbulence intensities incident to turbines 2 and 3 were decreased by 38% and 27%, respectively (full results in Supplementary Table 1). However, for $\alpha = 0°$ and $\gamma_1 = -20°$, where the wake is steered towards the downwind turbines as an intentionally suboptimal strategy in the fixed yaw experiment (Fig. 3a), the turbulence intensity incident to turbine 2 decreased by just 20% and the turbulence intensity incident to turbine 3 increased 4%. The standard individual wind turbine controller led to yaw activations (average amount of activations of yaw system during a 5 min time window), which were 29% of the maximum value recommended by the original equipment manufacturer (to limit fatigue loads and ensure normal turbine lifetime) for turbine 1, while wake steering increased this value to 38%, which is still significantly below the recommended threshold (Supplementary Figure 13). Finally, aeroelastic simulations suggest overall bending moment impacts between 0% and 5%, on average (that is, averaged over the full experimental window including periods of yaw alignment and misalignment depending on the inflow conditions, as in Fig. 5c) for the open-loop wind farm control strategy used in the energy maximization experiment. The potential impact of wake steering on fatigue loads is further discussed in Supplementary Note 4. Because wake steering can either increase or decrease turbine loads, future work should improve optimization-oriented load models that can be leveraged for multi-objective wind farm control optimization that maximizes energy and minimizes fatigue. The field experimental data presented in this study can be used to validate future models for the determinants of fatigue loads.

Conclusions

We demonstrate the potential for collective wind farm control at utility scale. In this study, we develop a predictive physics-based, data-assisted wind farm flow control model. To validate the model, we design a multi-month field experiment at a utility-scale wind farm. We demonstrate that the optimization-oriented flow control model is able to predict the yaw-misalignment angles that maximize the utility-scale wind turbine array power production within $\pm 5°$ for most conditions and the correct yaw-misalignment direction for all wind conditions.

We design a wake steering strategy by maximizing the power production of the wind turbine array depending on the incident atmospheric conditions in the validated model. For wind directions for which wake steering control is active and Region II wind speeds, the array energy production is increased by $3.0\% \pm 0.7\%$. For the same wind directions, considering the full wind speed range (including when wake steering is not active at high winds), the energy gain is $1.2\% \pm 0.4\%$. For Region II wind speeds, the energy gain across all incident wind directions is $1.1\% \pm 0.4\%$. Finally, for all wind speeds and directions, the energy gain is $0.4\% \pm 0.3\%$.

The gain in energy production at a commercial wind farm depends on the farm layout and the site-specific wind conditions. Given the incident winds observed during this experiment at the Indian farm, the energy gain is 1.1% and 0.4% for Region II and all wind speeds respectively. For wind generation to produce a larger fraction of energy worldwide, wind farm development will have to expand to onshore regions of lower mean wind speed and offshore environments, where wake losses are anticipated to be higher[43]. In this study, we demonstrate that wake steering control is a mechanism by which wind farm energy can be increased. We also demonstrate that the proposed flow control modelling framework is able to accurately predict the relative gain in power production from wake steering (model predictions are within the 95% confidence intervals of the field data for 72% (46/64) of the considered wind direction and yaw-misalignment cases), enabling its use in wind farm control and potentially in farm design[44].

Further improvements in active wake control are necessary to increase the efficacy of wake steering, such as closed-loop control[21,27,35,45] or machine learning-based methods[46]. Future research to develop wind farm flow control methodologies that jointly maximize wind farm energy production and minimize loads can further advance the implementation of collective control. Additionally, further improvements in flow control models are necessary to capture three-dimensional effects such as wake curling[37–39], veer[16,40] and stability[21,41] and to improve computationally efficient wind turbine fatigue load models[18,47].

To achieve climate goals, renewables must produce most of the demanded global energy. Wake steering is especially effective at increasing farm production at low wind speeds. Because annual wind speeds in India and other emerging economies are relatively low[48], wake steering is a promising mechanism to increase renewable energy production. Beyond higher annual energy production, low-carbon grids will require more predictable and controllable wind energy with reduced intermittency. Wake steering contributes to our ability to actively control the production from wind farms. Improvements in our ability to model, control and design wind energy generation will facilitate a more rapid energy grid decarbonization.

Methods

Predictive wind farm flow control model. With the goal of selecting the operational strategy for utility-scale wind turbines which maximizes energy production, we develop a wind farm flow control model that accounts for the variable atmospheric conditions. To remain tractable for controls-oriented modelling, the wind farm flow model must be computationally efficient[49]. But the model must be sufficiently accurate to ensure that the model-optimal yaw angles are closely representing the true power-maximizing yaw angles in complex field conditions.

In wind farms, there are limited sensors that measure the freestream wind flow at multiple heights (Fig. 1). Sensors that measure the wind flow up to the wind turbine hub height, which is approximately 100 m in altitude, are expensive[11]. Such sensors tend to be placed sparsely and suboptimally in wind farms[50] and are useful only for measuring the incident wind profiles, rather than velocities in turbine wakes. In summary, we generally have access to the incident wind profile through LiDAR or meteorological tower measurements, but we require a wake model to predict the wind flow field in the wake of turbines as a function of their operational strategy (Fig. 1). Further discussion of the role of the atmospheric conditions on the wind farm power is given in Supplementary Note 1.

We model the power production of yaw-misaligned wind turbines given the incident wind conditions using blade element theory. We denote the modelled power of upwind (unwaked) turbines as $\hat{P}_u$. Previous approaches have used a tuned empirical model to estimate the power production of yaw-misaligned turbines, where the power of the yaw-misaligned turbine is estimated as $\hat{P}_u(\gamma) = \hat{P}_u(\gamma = 0) \cdot \cos^{P_p}(\gamma)$, where P_p is a tuned parameter[24]. This empirical approach leads to substantial errors depending on the incident winds in the ABL[16]. Given variations in the wind speed and direction as a function of height z in the

ABL, we calculate the forces on the blade at each location in the wind turbine rotor area as a function of the radial r and azimuthal θ positions (schematic of the model shown in Supplementary Fig. 1). The wind turbine power production is modelled as the integration of the incremental torque over the rotor area multiplied by the angular velocity

$$\hat{P}_u = \Omega \int_0^{2\pi} \int_0^R r df_\tau(r, \theta), \quad (1)$$

where Ω is the blade angular velocity, R is the rotor radius and df_τ is the tangential force at a particular blade section. The tangential forces depend on characteristics of the wind turbine, including aerodynamic properties of the blades, the imposed yaw misalignment and the incident wind profiles[16]. The coefficients of lift and drag for the turbines of interest were provided by the manufacturer. More details on the power–yaw model are provided in Supplementary Methods.

We model the power production of downwind, waked turbines ($\hat{\boldsymbol{P}}_w$)using a computationally efficient analytical wake model developed by Howland et al.[19], which is based on a lifting line wake deflection model[34]. The full wake model is described in Supplementary Methods. We leverage modified linear wake superposition and an analytical secondary steering model[51], which models the effect of the non-zero lateral velocity at turbines downwind of a yawed turbine[52]. To predict wind turbine power production in a computationally efficient fashion, analytical wake models parameterize wake and ABL turbulence with an unknown wake spreading rate k_w[10,21,25]. Traditional approaches have tuned the wake model parameter to idealized data from simulations[53], which neglects the site-specific effects on the model parameters[19] and the effects of the stability of the ABL[21]. Instead, we estimate the wake model parameters using optimization-based inverse problem techniques[54], where we minimize the mean squared difference between the model predictions and field calibration data

$$\boldsymbol{k}_w^* = \arg\min \overline{(\hat{\boldsymbol{P}}_w(\boldsymbol{k}_w, \boldsymbol{\gamma}=0) - \boldsymbol{P}_w(\boldsymbol{\gamma}=0))^2}. \quad (2)$$

We calibrate the wake spreading rate and the proportionality constant of the presumed Gaussian wake using an offline variant of the ensemble Kalman filter[21,35,55] (Supplementary Methods). The calibration leverages site- and wind condition-specific historical data collected where the wind farm is in standard individual operation ($\gamma=0$). The wake model parameters are calibrated for each wind condition bin, considering wind speed, wind direction and turbulence intensity. The calibrated model parameters are then used to predict the power production for the wind farm in wake steering configurations ($\gamma\neq0$). The power-maximizing wind farm control strategy with N_t turbines is predicted using the flow control model as

$$\boldsymbol{\gamma}^* = \arg\max \sum_{i=1}^{N_t} \hat{P}_i(\boldsymbol{\gamma}). \quad (3)$$

We estimate γ^* using gradient-based optimization of the flow control model[19] for each wind condition bin. More details regarding the set point optimization are provided in Supplementary Note 2.

Experimental setup. We record data from each turbine in the form of 1 min averaged Supervisory Control and Data Acquisition data, which includes power production, nacelle position, blade pitch and other relevant turbine variables. The wind profiles depending on height are recorded in 1 min averages using a Leosphere Windcube V2.0 profiling LiDAR on site.

Fixed yaw-misalignment experiment data filtering. For the fixed yaw-misalignment experiment, turbine 1 (Fig. 2b) implements a yaw-misalignment set point sequence between $\gamma=-25°$ and $+25°$ (Fig. 2d). The yaw-misalignment set points are active for Region II wind speeds, between approximately 5 m s^{-1} and 9 m s^{-1}. Because the wind direction in the ABL is constantly evolving, the standard wind turbine yaw control system is used to track the yaw-misalignment set point[36]. The yaw set point tracking ability of the turbine model of interest was validated by Howland et al.[16]. Data are aggregated in 1 min averages. We consider data only in which all four turbines (three test turbines and reference turbine) are active and operating normally.

For the fixed yaw-misalignment experiment, we consider conditional averages of the power ratio for the turbines of interest. We characterize the freestream wind conditions using measurements made by the reference turbine (Fig. 2b). We focus on wind speeds between 5.5 m s^{-1} and 8.5 m s^{-1}. Because the wake interactions depend on the turbulence intensity[21], we restrict the analysis to turbulence intensities between 2.5% and 7.5%. We characterize the realized yaw misalignment of turbine 1 based on the nacelle-mounted measurements of the relative wind direction of turbine 1, measured by a sonic anemometer. We consider yaw misalignment for values between −25° and 25° with a step size of 5°. The wind direction is considered for values between −10° and 2.5° with a step size of 2.5°.

Energy gain analysis methodology. To estimate the impact of the wake steering control on energy production, we compute the energy ratio, which is the ratio of the energy production of the test turbine of interest to the energy production of the reference turbine. The energy ratio is given by

$$E_r = \frac{\sum_{i=1}^{N_b} w_i \overline{P}_i^{\text{test}}}{\sum_{i=1}^{N_b} w_i \overline{P}_i^{\text{ref}}}, \quad (4)$$

where N_b is the number of wind speed bins, w_i is the wind condition-specific weighting factor and $\overline{P}$ is the mean power production within the particular wind speed bin. The energy ratio is computed for each wind direction. Additionally, the energy ratio is computed for both baseline yaw-aligned control (base) and for wake steering control (steer). Because the experimental window is finite, the wind condition distributions between collective and standard control are not identical[30]. To account for this, the weighting factors are defined using the number of samples from both control strategies

$$w_i^{\text{base}} = \frac{n_i^{\text{base}} + n_i^{\text{steer}}}{N^{\text{base}} + N^{\text{steer}}} \qquad w_i^{\text{steer}} = \frac{n_i^{\text{base}} + n_i^{\text{steer}}}{N^{\text{base}} + N^{\text{steer}}}, \quad (5)$$

where w_i^{base} and w_i^{steer} are the weights (w_i) used in the energy ratio calculation for the baseline yaw-aligned and the wake steering cases, respectively. The number of samples in the wind speed bin for a particular wind direction is given by n_i. The number of total samples for a particular wind direction is given by N. We test the influence of different weighting approaches in Supplementary Note 5 (Supplementary Table 2). We find that the different weighting methods do not have a statistically significant impact on our energy gain results. The fractional gain in energy for each wind direction is

$$R = \frac{E_r^{\text{steer}}}{E_r^{\text{base}}}. \quad (6)$$

The influence of wake steering on the energy production over a sector of wind directions can be approximated using the energy ratio. The sector energy gain is

$$G_r = \sum_{i=1}^{N_a} W_i^{\text{ref}} R_i, \quad (7)$$

where N_a is the number of wind directions considered in the sector energy analysis and R_i is the energy ratio gain for each wind direction (equation (6)). The weights are

$$W_i^{\text{ref}} = \frac{\overline{E}_i^{\text{ref}} N_i^{\text{ref}}}{\sum_{i=1}^{N_a} \overline{E}_i^{\text{ref}} N_i^{\text{ref}}}, \quad (8)$$

which represents the fraction of energy produced in each wind direction (accounting for the observed wind rose during the experiment). The averaged power produced by the reference turbine for each wind direction is $\overline{E}_i^{\text{ref}}$, and N_i^{ref} is the number of samples for each wind direction. Confidence intervals for each statistic are calculated using bootstrapping.

Farm energy maximization data filtering. For the wake steering farm energy maximization experiment, we switch between wake steering control and baseline yaw-aligned control with a period of 2.5 h. We selected a switching period of 2.5 h to balance the aim of collecting data in similar conditions while limiting the number of transitions between control strategies. When baseline yaw-aligned control is activated, all turbines implement a strategy of $\gamma=0°$. When wake steering is activated, turbines 1 and 2 implement a dynamic yaw-misalignment sequence based on the incident wind conditions (Fig. 5c), and turbine 3 implements a yaw-aligned strategy of $\gamma=0°$. As with the fixed yaw experiment, the standard wind turbine yaw control system is used to track the intended yaw-misalignment set point, which now varies as a function of the incident wind conditions. Data are aggregated in 1 min averages.

We compute the energy ratio (equation (4)) using the data for the two different control approaches (wake steering and baseline yaw aligned). We consider wind speed and direction ranges as specified by Table 1 with a step size of 1 m s^{-1}. We consider only wind directions with more than 20 data points in both control cases. We consider only wind speed subsets of a wind direction bin with more than five data points in both control cases. Because high turbulence was infrequent in these experiments and it gives high noise-to-signal ratio and turbine loads[18] and wake losses are minimal in inflow with high turbulence, turbulence intensities less than 20% are considered for wake steering. We consider data only in which all four turbines (three test turbines and reference turbine) are active and operating normally.

Data availability

All data generated or analysed during this study are included in the published article and its Supplementary Information. The data are available at: https://doi.org/10.5281/zenodo.6621555. Source data are provided with this paper.

Code availability

The code used during this study is provided in the Supplementary Software Files. Instructions for the code use are provided as examples and comments in the Supplementary Software Files. The code is available at: https://doi.org/10.5281/zenodo.6621555.

Received: 16 January 2022; Accepted: 27 June 2022;
Published online: 11 August 2022

References

1. IPCC *Climate Change 2021: The Physical Science Basis* (eds Masson-Delmotte, V. et al.) (Cambridge University Press, 2021).
2. IPCC *Special Report on Global Warming of 1.5 °C* (eds Masson-Delmotte, V. et al.) (Cambridge University Press, 2018).
3. Gielen, D. et al. The role of renewable energy in the global energy transformation. *Energy Strategy Rev.* **24**, 38–50 (2019).
4. *Fact Sheet: President Biden Sets 2030 Greenhouse Gas Pollution Reduction Target Aimed at Creating Good-Paying Union Jobs and Securing U.S. Leadership on Clean Energy Technologies* (White House, 2021); https://www.whitehouse.gov/briefing-room/statements-releases/2021/04/22/fact-sheet-president-biden-sets-2030-greenhouse-gas-pollution-reduction-target-aimed-at-creating-good-paying-union-jobs-and-securing-u-s-leadership-on-clean-energy-technologies
5. Renn, O. & Marshall, J. P. Coal, nuclear and renewable energy policies in Germany: from the 1950s to the 'energiewende'. *Energy Policy* **99**, 224–232 (2016).
6. Asif, M. & Muneer, T. Energy supply, its demand and security issues for developed and emerging economies. *Ren. Sust. Energy Rev.* **11**, 1388–1413 (2007).
7. Veers, P. et al. Grand challenges in the science of wind energy. *Science* **366**, eaau2027 (2019).
8. Wiser, R. et al. Wind vision: a new era for wind power in the United States. *Electr. J.* **28**, 120–132 (2015).
9. Barthelmie, R. J. et al. Modelling and measuring flow and wind turbine wakes in large wind farms offshore. *Wind Energy* **12**, 431–444 (2009).
10. Stevens, R. J. & Meneveau, C. Flow structure and turbulence in wind farms. *Annu. Rev. Fluid Mech.* **49**, 311–339 (2017).
11. Eberle, A., Roberts, J. O., Key, A., Bhaskar, P. & Dykes, K. L. *NREL's Balance-of-System Cost Model for Land-Based Wind, Technical Report* (National Renewable Energy Lab, 2019).
12. Stevens, R. J., Hobbs, B. F., Ramos, A. & Meneveau, C. Combining economic and fluid dynamic models to determine the optimal spacing in very large wind farms. *Wind Energy* **20**, 465–477 (2017).
13. Meyers, J. & Meneveau, C. Optimal turbine spacing in fully developed wind farm boundary layers. *Wind Energy* **15**, 305–317 (2012).
14. Pao, L. Y. & Johnson, K. E. A tutorial on the dynamics and control of wind turbines and wind farms. In *2009 American Control Conference* 2076–2089 (IEEE, 2009).
15. Fleming, P. et al. Field-test results using a nacelle-mounted lidar for improving wind turbine power capture by reducing yaw misalignment. *J. Phys. Conf. Ser.* **524**, 012002 (2014).
16. Howland, M. F. et al. Influence of atmospheric conditions on the power production of utility-scale wind turbines in yaw misalignment. *J. Ren. Sust. Energy* **12**, 063307 (2020).
17. Fleming, P. et al. Simulation comparison of wake mitigation control strategies for a two-turbine case. *Wind Energy* **18**, 2135–2143 (2015).
18. Damiani, R. et al. Assessment of wind turbine component loads under yaw-offset conditions. *Wind Energy Sci.* **3**, 173–189 (2018).
19. Howland, M. F., Lele, S. K. & Dabiri, J. O. Wind farm power optimization through wake steering. *Proc. Natl Acad. Sci. USA* **116**, 14495–14500 (2019).
20. Fleming, P. et al. Field test of wake steering at an offshore wind farm. *Wind Energy Sci.* **2**, 229–239 (2017).
21. Howland, M. F. et al. Optimal closed-loop wake steering–part 2: diurnal cycle atmospheric boundary layer conditions. *Wind Energy Sci.* **7**, 345–365 (2022).
22. Quick, J. et al. Optimization under uncertainty for wake steering strategies. *J. Phys. Conf. Ser.* **854**, 012036 (2017).
23. Choi, H. & Moin, P. Grid-point requirements for large eddy simulation: Chapman's estimates revisited. *Phys. Fluids* **24**, 011702 (2012).
24. Gebraad, P. et al. Wind plant power optimization through yaw control using a parametric model for wake effects—a CFD simulation study. *Wind Energy* **19**, 95–114 (2016).
25. Meneveau, C. Big wind power: seven questions for turbulence research. *J. Turbul.* **20**, 2–20 (2019).
26. Howland, M. F. Wind farm yaw control set-point optimization under model parameter uncertainty. *J. Ren. Sust. Energy* **13**, 043303 (2021).
27. Doekemeijer, B. M., van der Hoek, D. & van Wingerden, J.-W. Closed-loop model-based wind farm control using floris under time-varying inflow conditions. *Ren. Energy* **156**, 719–730 (2020).
28. Bastankhah, M. & Porté-Agel, F. Wind farm power optimization via yaw angle control: a wind tunnel study. *J. Ren. Sust. Energy* **11**, 023301 (2019).
29. Campagnolo, F., Weber, R., Schreiber, J. & Bottasso, C. L. Wind tunnel testing of wake steering with dynamic wind direction changes. *Wind Energy Sci.* **5**, 1273–1295 (2020).
30. Fleming, P. et al. Initial results from a field campaign of wake steering applied at a commercial wind farm–part 1. *Wind Energy Sci.* **4**, 273–285 (2019).
31. Doekemeijer, B. M. et al. Field experiment for open-loop yaw-based wake steering at a commercial onshore wind farm in italy. *Wind Energy Sci.* **6**, 159–176 (2021).
32. Fleming, P. et al. Experimental results of wake steering using fixed angles. *Wind Energy Sci.* **6**, 1521–1531 (2021).
33. Bastankhah, M. & Porté-Agel, F. A new analytical model for wind-turbine wakes. *Ren. Energy* **70**, 116–123 (2014).
34. Shapiro, C. R., Gayme, D. F. & Meneveau, C. Modelling yawed wind turbine wakes: a lifting line approach. *J. Fluid Mech.* **841**, R1 (2018).
35. Howland, M. F., Ghate, A. S., Lele, S. K. & Dabiri, J. O. Optimal closed-loop wake steering–part 1: conventionally neutral atmospheric boundary layer conditions. *Wind Energy Sci.* **5**, 1315–1338 (2020).
36. Burton, T., Jenkins, N., Sharpe, D. & Bossanyi, E. *Wind Energy Handbook* (John Wiley & Sons, 2011).
37. Howland, M. F., Bossuyt, J., Martínez-Tossas, L. A., Meyers, J. & Meneveau, C. Wake structure in actuator disk models of wind turbines in yaw under uniform inflow conditions. *J. Ren. Sust. Energy* **8**, 043301 (2016).
38. Martínez-Tossas, L. A. et al. The curled wake model: a three-dimensional and extremely fast steady-state wake solver for wind plant flows. *Wind Energy Sci.* **6**, 555–570 (2021).
39. Bastankhah, M., Welch, B. L., Martínez-Tossas, L. A., King, J. & Fleming, P. Analytical solution for the cumulative wake of wind turbines in wind farms. *J. Fluid Mech.* **911**, A53 (2021).
40. Abkar, M., Sørensen, J. N. & Porté-Agel, F. An analytical model for the effect of vertical wind veer on wind turbine wakes. *Energies* **11**, 1838 (2018).
41. Peña, A., Réthoré, P.-E. & Rathmann, O. Modeling large offshore wind farms under different atmospheric stability regimes with the park wake model. *Ren. Energy* **70**, 164–171 (2014).
42. Frandsen, S. *Turbulence and Turbulence-Generated Structural Loading in Wind Turbine Clusters*. PhD thesis, Technical University of Denmark (2007).
43. Bodini, N., Lundquist, J. K. & Kirincich, A. U.S. East Coast Lidar measurements show offshore wind turbines will encounter very low atmospheric turbulence. *Geophys. Res. Lett.* **46**, 5582–5591 (2019).
44. Fleming, P. A., Ning, A., Gebraad, P. M. & Dykes, K. Wind plant system engineering through optimization of layout and yaw control. *Wind Energy* **19**, 329–344 (2016).
45. Ciri, U., Rotea, M. A. & Leonardi, S. Model-free control of wind farms: a comparative study between individual and coordinated extremum seeking. *Ren. Energy* **113**, 1033–1045 (2017).
46. Stanfel, P., Johnson, K., Bay, C. J. & King, J. Proof-of-concept of a reinforcement learning framework for wind farm energy capture maximization in time-varying wind. *J. Ren. Sust. Energy* **13**, 043305 (2021).
47. Hulsman, P., Andersen, S. J. & Göçmen, T. Optimizing wind farm control through wake steering using surrogate models based on high-fidelity simulations. *Wind Energy Sci.* **5**, 309–329 (2020).
48. Purohit, I. & Purohit, P. Wind energy in India: status and future prospects. *J. Ren. Sust. Energy* **1**, 042701 (2009).
49. Boersma, S., Gebraad, P., Vali, M., Doekemeijer, B. & Van Wingerden, J. A control-oriented dynamic wind farm flow model: 'wfsim'. *J. Phys. Conf. Ser.* **753**, 032005 (2016).
50. Annoni, J. et al. Sparse-sensor placement for wind farm control. *J. Phys. Conf. Ser.* **1037**, 032019 (2018).
51. Howland, M. F. & Dabiri, J. O. Influence of wake model superposition and secondary steering on model-based wake steering control with scada data assimilation. *Energies* **14**, 52 (2021).
52. King, J. et al. Controls-oriented model for secondary effects of wake steering. *Wind Energy Sci.* **6**, 701–714 (2021).
53. Niayifar, A. & Porté-Agel, F. Analytical modeling of wind farms: a new approach for power prediction. *Energies* **9**, 741 (2016).
54. Stuart, A. M. Inverse problems: a Bayesian perspective. *Acta Numer.* **19**, 451–559 (2010).
55. Evensen, G. The ensemble kalman filter: theoretical formulation and practical implementation. *Ocean Dyn.* **53**, 343–367 (2003).

Acknowledgements

We would like to thank the field site team from ReNew Power who assisted with the experiment. M.F.H. acknowledges partial support from the MIT Energy Initiative and Siemens Gamesa Renewable Energy. J.O.D. acknowledges partial support from the California Institute of Technology. The authors would like to thank the reviewers for their thoughtful comments and contribution to this work. We would also like to thank G. Tregnago for thoughtful comments and contribution to this work.

Author contributions

M.F.H., V.S. and J.O.D. conceived the research. M.F.H. developed the flow control model and code and analysed the data. J.B.Q., J.J.P.M. and F.P.L. implemented the yaw offsets, provided feedback and suggestions on the flow control model and contributed codes for data analysis. N.Y. and J.S.C. performed LiDAR installation and wind farm site management. M.F.H. wrote the manuscript. All authors contributed to manuscript edits.

Competing interests

The authors declare no competing interests.

Additional information

Supplementary information The online version contains supplementary material available at https://doi.org/10.1038/s41560-022-01085-8.

Correspondence and requests for materials should be addressed to Michael F. Howland.

Peer review information *Nature Energy* thanks Maarten Paul van der Laan and Eric Simley for their contribution to the peer review of this work.